Plasma Chem Plasma Process (2014) 34:767–784
DOI 10.1007/s11090-014-9531-7

ORIGINAL PAPER

Nanocrystalline Diamond Thin Films Synthesis on Curved Surface

Duosheng Li · Qing H. Qin · Dunwen Zuo · R. W. Boswell · Wenzhuang Lu · Zbigniew Stachurski

Received: 10 October 2013 / Accepted: 7 February 2014 / Published online: 22 February 2014

Abstract Thin films of curved surface nanocrystalline diamond (CS-NCD) are a category of important materials. However, the development of such materials is still a highly challenging task. Here we present a novel approach to synthesizing CS-NCD thin films deposited on non-spherical surfaces of molybdenum substrate using direct current plasma jet chemical vapor deposition. A special cooling system was designed and applied to ensure uniform substrate temperature. It is demonstrated from simulation and experimental results that this system is favorable for the production of thin films. The results show that the quality of CS-NCD thin films depends on the selection of optimal values of parameters including CH_4 concentration, substrate temperature, and chamber pressure. If the CH_4 concentration and/or the substrate temperature is too high or low, it results in non-diamond phase or micron-crystalline diamond thin films. Synthetic CS-NCD thin films using the proposed method have a smooth surface and uniform thickness. The average grain size and the mean surface roughness are approximately 30 and 4.3 nm respectively. Characteristics of CS-NCD thin film spectra comprised of the full width at half maximum with broad Raman peaks around 1,140 and 1,480 cm^{-1}, confirming the presence of the NCD phase.

Keywords Chemical vapor deposition · Characterization · Curved surface nanocrystalline diamond · Thin film · Morphology

D. Li (✉)
School of Material Science and Engineering, Nanchang Hangkong University, Nanchang 330063, China
e-mail: ldsnuaa@nuaa.edu.cn

D. Li · Q. H. Qin · Z. Stachurski
Research School of Engineering, Australian National University, Canberra, ACT 0200, Australia

D. Zuo · W. Lu
Department of Mechanical and Electrical Engineering, Nanjing University of Aeronautics and Astronautics, Nanjing 210016, China

R. W. Boswell
Research School of Physics, Australian National University, Canberra, ACT 0200, Australia

Introduction

Nanocrystalline diamond (NCD) thin films possess outstanding properties such as low threshold for field emission, high surface smoothness and hardness, excellent biocompatibility, high thermal conductivity, and low friction coefficient [1–4]. They have been synthesized by various CVD technologies, such as DCPJCVD [5, 6], Pulsed laser deposition (PLD) [7], hot filament CVD (HF-CVD) [8], and microwave plasma CVD (MW-CVD) [9, 10]. Synthetic NCD thin films are usually flat and wafer-like [11]. For example, Zhou [12] prepared NCD thin film by MW-CVD, and Meng [13] prepared NCD thin film on cemented carbide using a high extended DC arc plasma process with high current. Morell [14] investigated the synthesis, microstructure, and field emission properties of sulfur-doped NCD by HF-CVD. During the past decade, CS-NCD thin films have attracted widespread attention due to their promising applications as semiconductor, biomaterial, microwave optical window of high speed flight heat-seeking missile dome, and coating machining tools, cold-cathode electron sources and micro- and nano-electromechanical systems [15]. To the authors' knowledge, however, there has been no report of growing CS-NCD thin film on non-spherical surface molybdenum (Mo) substrate. Huang and Lunn [16, 17] only synthesized small size micron level curved surface diamond thin films by HF-CVD. This might be due to the synthesizing process being very sophisticated, as it is particularly difficult to maintain a constant temperature distribution over the whole curved surface substrate. The consequence of non-uniform temperature distribution may be significant residual stress and impurity in CS-NCD thin film. It may also have negative impacts on both the quality and the grain size of the film.

As an alternative to the experimental approach, computer simulation study of the growth process of diamond film is an increasingly useful method due to its low cost, high efficiency and reproducibility [18]. To authors' knowledge, most simulation reports have been based on micro-Monte Carlo and molecular dynamics [19, 20]. They are powerful for describing the growth of NCD thin films. However, these methods are inconvenient and inefficient for simulating surface temperature and mass flow in the synthesizing process. In general, CS-NCD thin films can grow on heterogeneous substrates such as Mo, Si, and cemented carbide alloy. Considering that both the coefficient of thermal expansion (CTE) and the lattice constant of diamond are significantly different from those of the substrate, it is more difficult to grow CS-NCD thin films on curved substrates than on planar substrates. In this paper, a synthetic process for depositing CS-NCD thin films on non-spherical surfaces is reported and the properties of the films are characterized using atom force microscopy (AFM, SPM-9600), field emission scanning electron microscopy (FE-SEM, JSM-6700F), Raman spectroscopy (LABRAM-HR), and roughness-profile metering (MMD-100). AFM is a form of scanning probe microscopy. It works by scanning an extremely fine probe at the end of a cantilever across the surface of a material, which can provide a 3D profile of the surface and much more topographical information than optical or scanning electron microscopes. FE-SEM is used to visualize very small topographic details on the surface of materials. Researchers employ this technique to observe the microstructure of materials that may be as thin as 1 nm. Raman spectroscopy is a proven and very important non-destructive characterization technique for distinguishing micro-sized particles of C-polymorphs, as it is very sensitive to the nature of carbon bonding. A typical application is in situ identification of inclusions of C-polymorphs (diamond–graphite) in CS-NCD.

Experimental Set-Up and Procedure

Experimental Set-Up

A modified LP-30 direct current plasma jet CVD system was used to synthesize CS-NCD thin films on a curved substrate. The schematic diagram is shown in Fig. 1. It includes a mixed gas input system, a cooling system, an electrical system and a plasma torch. In the CVD system, a particular DC arc plasma torch is employed. The torch is a magnetic and fluid dynamically controlled, large orifice, and long discharge tunnel plasma torch. To stabilize the plasma arc an external magnetic field is applied, which rotates the plasma arc and forms uniform and stable plasma fluid to coat the substrate surface evenly. The plasma torch consists of a rod-like cathode, which is usually made of tungsten alloy, and a circular-ring anode made of oxygen-free copper. A novel cooling water recycling system has been designed to cool the CVD system [21].

Experimental Procedure

Curved surface nanocrystalline diamond (CS-NCD) thin films were formed by depositing the particles on the non-spherical surface of Mo substrate as shown in Fig. 1. Mo was adopted as the substrate because its crystal structure is similar to that of diamond, and thus CS-NCD thin film can grow easily on a Mo substrate. The substrate temperature was measured using an optical infrared pyrometer, and the temperature signal was transmitted to a computer which issued directions to control both the plasma torch power and the flow rate of cooling water. The substrate temperature could thus be precisely controlled. Before the CS-NCD thin films were grown, the Mo substrate was pretreated by diamond powder pre-polishing and ultrasonic cleaning, with a suspension of 0.1–30 μm diamond powder in ethanol and atomic hydrogen etching respectively. When the films began to grow, the reaction chamber was injected with a pure argon and reactive gas mixture consisting of argon (Ar), high-pure (99.99 %) methane (CH_4), and hydrogen (H_2). The total gas mixture pressure was kept at 50–60 Torr. The CH_4 concentration was 1.0–10.0 %. The substrate temperature was in the range of 830–1,150 °C. By controlling the CH_4 concentration and the deposition time at 25–50 min, the CS-NCD thin films were allowed to grow to about 1 micron thickness. The other experimental ambient conditions have been described in detail elsewhere [22]. FE-SEM, AFM, roughness-profile metering, and Raman spectroscopy were used to characterize the microstructure, internal quality, and surface morphology of the CS-NCD thin films.

A Novel Cooling System Designation

Uniform temperature distribution of the curved surface substrate is crucial for the growth of CS-NCD thin films. Any temperature fluctuation of the substrate can induce non-tolerant residual stress in CS-NCD thin films. Such non-tolerant residual stress can even result in rupture of the film, or the diamond thin film may contain impurities such as graphite or amorphous carbon. It is difficult to maintain a constant temperature over the whole curved surface substrate using existing cooling systems. Indeed, in our previous experiments, we have found that synthetic CS-NCD contain many impurities and defects. This is due to the center area temperature of the substrate being 10 % higher than that at the edge. To overcome this problem, we designed a new cooling system incorporating the following aspects:

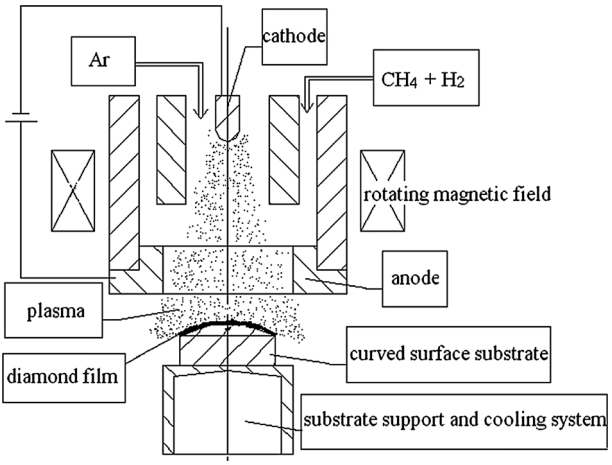

Fig. 1 Schematic diagram of the direct current jet plasma vapor deposition system

1. The curved surface substrate was laid on a copper base with good thermal conductivity.
2. A circulating cooling channel was installed on the base of copper, to control the wall thickness of the copper base. The thickness of the copper base is assumed to be inversely proportional to the distribution of the substrate temperature; in other words, the higher the substrate temperature, the thinner the wall thickness of the copper base is. A thinner copper base has a higher cooling rate and takes more heat away from the substrate.
3. The copper base wall is in contact with the curved surface substrate when it is produced (see Fig. 2). Therefore its curve should theoretically be the same as that of the curved surface. To make the manufacturing process tractable, the copper base was formed in a stepwise ring structure or a spherical structure (see Fig. 2), which approximately matched the surface shape of the substrate (either convex or concave surface structure).
4. During the deposition process, the cooling system continuously injects water to keep the substrate cool. The temperature variation of the substrate surface is controlled within the range of 0.6–1.5 % of the maximum temperature.

Figure 2 shows the design of the cooling system of the curved surface substrate based on the description above. A cooling system with a convex surface substrate is shown in Fig. 2a and one with a concave surface substrate system is shown in Fig. 2b. It contains a copper base (indicated by 6 or 12 in Fig. 2), and its upper surface is in contact with the lower surface of the substrate (1 or 7 in Fig. 2). The copper base is a hollow curved structure. The function of component 2 or 8 in Fig. 2 is to distribute circulating water to the whole system, and for this purpose it is installed under the copper base. Component 2 or 8 contains nine inlet channels (3 or 9 in Fig. 2) and eight outlet channels (4 or 10 in Fig. 2). There is a cooling water chamber (5 or 11 in Fig. 2) between the copper base and component 2 or 8. To ensure that sufficient cooling water remains in 5 or 11 and effectively implements the heat exchange with the copper base, the hole size of the inlet channel (3 or 9 in Fig. 2) should be larger than that of the outlet channel (4 or 10 in Fig. 2).

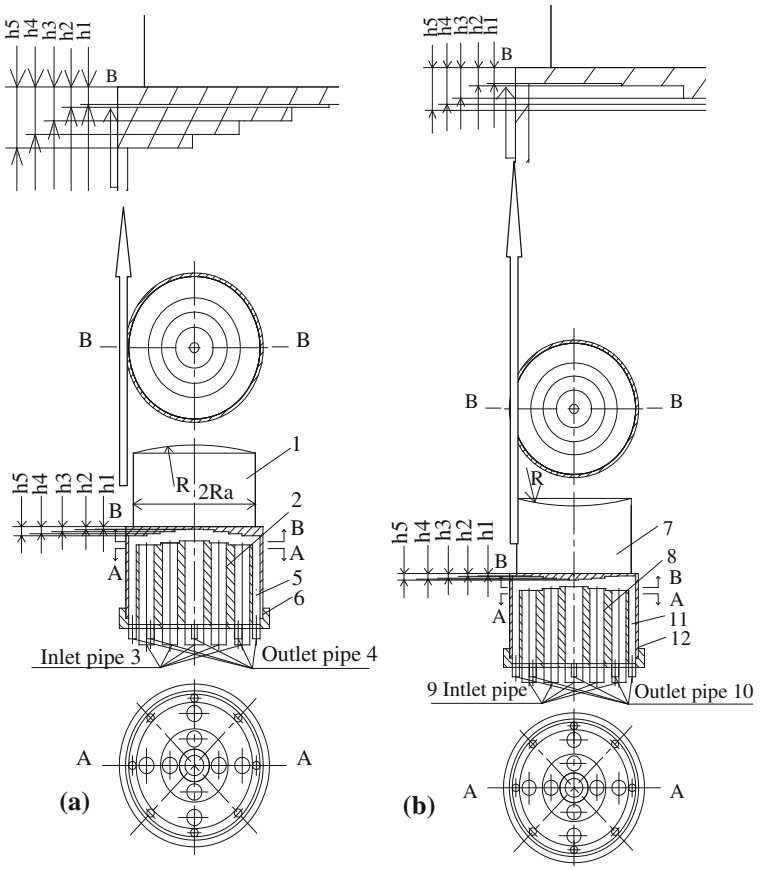

Fig. 2 Cooling system of curved surface substrate, **a** convex surface substrate cooling system, **b** concave surface substrate system

The inner surface on the top of the wall of cooling water chamber 5 or 11 is in contact with substrate 1 or 7. It has the same radius as the curved surface substrate. The surface temperature distribution of the substrate varies inversely with the wall thickness of the cooling water chamber. In other words, a higher temperature region of the curved surface substrate corresponds to a smaller wall thickness.

The new cooling system is shown in Fig. 2. The wall thickness *hi* (i = 1–5) (see Fig. 2) of the copper base is determined using the following equations:

$$\mathrm{h1} = 0.0004\mathrm{R} + 1.3563 \tag{1}$$

$$\mathrm{h2} = -0.0001\mathrm{R}^2 + 0.0046\mathrm{R} + 1.8674 \tag{2}$$

$$\mathrm{h3} = -0.0051\mathrm{R} + 2.8717 \tag{3}$$

$$\mathrm{h4} = -0.0027\mathrm{R} + 3.9076 \tag{4}$$

$$\mathrm{h5} = 0.0001\mathrm{R}^2 - 0.0118\mathrm{R} + 5.1713 \tag{5}$$

where R is radius of the curved surface of the substrate, and h1–h5 are shown in Fig. 2.

Results and Discussion

Numerical Simulation Using Finite Element Method

In this section, fields of temperature and mass transfer during the synthesis process are simulated using finite element method. The physical model of CS-NCD used in the calculation is based on the following assumptions: (1) DC plasma is an ideal plasma and the distributions of velocity and pressure are assumed to satisfy Maxwell's equations (2) the temperature of ionized atoms is assumed to be approximately equal to the temperature of atoms (3) the Spalart–Allmaras nonlinear equations are used to simulate the thermal dynamic process of the plasma jet. In the analysis, the DC plasma flow is regarded as a stationary fluid. Thus, the assumption of Spalart–Allmaras flow can be used in the present flow problem. The deposition chamber is simplified for modeling the process using the following equations. The synthesizing process of CS-NCD thin films satisfies the mass conservation equation, momentum conservation equation, and energy conservation equation [23].

Basic Equations for Mass Transfer

The mass increase of the fluid micro unit per unit time is equal to the flow of the net mass into the domain of the micro-element in the same time interval. The mass conservation equation of the problem is written as:

$$\frac{\partial \rho}{\partial t} + \frac{\partial(\rho u)}{\partial x} + \frac{\partial(\rho v)}{\partial y} + \frac{\partial(\rho w)}{\partial z} = 0 \tag{6}$$

Making use of vector symbol $div(a) = \partial a_x/\partial x + \partial a_y/\partial y + \partial a_z/\partial z$, Eq. (6) can be simplified as

$$\frac{\partial \rho}{\partial t} + div(\rho U) = 0 \tag{7}$$

where ρ is the mass density, t is the time variable, U (=$\{u, v, w\}$) is the velocity vector, u, v, and w are the components of the velocity U in the x, y, and z directions respectively.

The rate of change of momentum of the fluid in a micro-element is equal to the total of external forces loading the domain of the micro-element. The momentum conservation equation can then be written as:

$$\frac{\partial(\rho u)}{\partial t} + div(\rho u U) = -\frac{\partial p}{\partial x} + \frac{\partial \tau_{xx}}{\partial x} + \frac{\partial \tau_{yx}}{\partial y} + \frac{\partial \tau_{zx}}{\partial z} + F_x \tag{8}$$

$$\frac{\partial(\rho v)}{\partial t} + div(\rho v U) = -\frac{\partial p}{\partial y} + \frac{\partial \tau_{xy}}{\partial x} + \frac{\partial \tau_{yy}}{\partial y} + \frac{\partial \tau_{zy}}{\partial z} + F_y \tag{9}$$

$$\frac{\partial(\rho w)}{\partial t} + div(\rho w U) = -\frac{\partial p}{\partial x} + \frac{\partial \tau_{xz}}{\partial x} + \frac{\partial \tau_{yz}}{\partial y} + \frac{\partial \tau_{zz}}{\partial z} + F_z \tag{10}$$

where p is pressure of the fluid micro-cell, τ_{xy} τ_{xy} andτ_{xz} are viscous stress components of the micro-surfaces due to molecular viscous effects, Fx, Fy, and Fz are the body forces of the micro-cell in the x, y, and z directions respectively.

Basic Equations for Heat Transfer

The experiment involves the flow system of heat exchange, which complies with the energy conservation law. The energy E of a fluid usually consists of internal energy E_i, kinetic energy $K = (u^2 + v^2 + w^2)/2$, and potential energy P. The internal energy E_i is a function of the temperature T, i.e. $E_i = C_P T$; meanwhile, the total energy E is also a function of the temperature T. Eq. (11) represents the energy conservation equations.

$$\frac{\partial(\rho T)}{\partial t} + div(\rho UT) = div\left(\frac{k}{c_p} gradT\right) + S_T \tag{11}$$

Eq. (11) can be written in expanded form as follows:

$$\frac{\partial(\rho T)}{\partial t} + \frac{\partial(\rho uT)}{\partial x} + \frac{\partial(\rho vT)}{\partial y} + \frac{\partial(\rho wT)}{\partial z} = \frac{\partial}{\partial x}\left(\frac{k}{c_p}\frac{\partial T}{\partial x}\right) + \frac{\partial}{\partial y}\left(\frac{k}{c_p}\frac{\partial T}{\partial y}\right) + \frac{\partial}{\partial z}\left(\frac{k}{c_p}\frac{\partial T}{\partial z}\right) + S_T \tag{12}$$

where c_p is the specific heat capacity, T is temperature, k is the heat transfer coefficient of the fluid, S_T is the internal heat source of the fluid due to fluid mechanical energy being sometimes converted to heat energy by the viscous effect, and is termed viscous dissipation. The simplified heat transfer coefficient k (W/m^2 °C) of water cooling is given by

$$k = \frac{Q}{A(T_S - T_w)} = \frac{q\rho\ c_w(T_2 - T_1)}{A(T_S - T_w)} \tag{13}$$

where A is the area of contact (m^2) with water at the bottom of the substrate; T_S is temperature (°C) over the bottom of the substrate; T_w is the temperature (°C) of the water on the surface of the substrate, Q is the heat flux (W); q is the cooling water flow rate (m^3/s); ρ is the water density (kg/m^3); c_w is the water heat capacity (J/(kg °C); T_1 is the inlet temperature of the cooling water (°C); T_2 is the outlet temperature (°C) of the cooling water. The rate of water flow is measured by flow rate sensor, and the flow rate signal is transmitted to a computer which issues a directive to control the flow rate of cooling water, producing a heat exchange coefficient of 10–20 KW/(m^2 °C) between the cooling water and the copper base.

Numerical Simulation by Finite Element Method

Numerical solutions for Eqs. (6)–(12) can be obtained using the well-known finite element method [24–27]. In the following, finite element results for temperature field and mass transfer are presented to verify the experimental observations.

In the calculation, the following aspects are considered. During the deposition process, the main component of the reaction gas is hydrogen, and the volume ratio of H_2 is 90–99 %, while the proportion of methane is only 1–10 %. The total flow of the gas is 9,500 sccm. The gas mixture flows into the reaction chamber from the anode nozzle with a diameter of 76 mm. After the gas pressure in the reaction chamber reaches stability, the entrance pressure is 0.1 MPa, the gas outlet pressure is 4.5–5.0 kPa, the gas flow rate is 4.5–5.0 m s^{-1}, and the temperature is in the range of 7,000–10,000 K. Physical parameters of the materials are presented in Table 1. The finite element results of mass transfer and temperature simulation on the curved surface substrate are shown in Figs. 3 and 4, respectively.

Table 1 Physical parameters of materials

Materials	Density (kg/m^3)	Specific heat (J/kg K)	Thermal conductivity (W/m K)	Viscosity (kg/m s)
Gas mixture	0.7693	8101.07	0.09918	$1.40815e^{-05}$
Mo	10,200	251	137	–
304	8,030	502.48	16.27	–

Figure 3 shows the finite element results of pressure, temperature, and velocity distributions for three radii of curvature of the convex substrate (R): 134, 108, and 91 mm respectively. The corresponding visualized pressure distributions are shown in Fig. 3a, d, g, visualized velocity distributions in Fig. 3b, e, f, and visualized temperature distributions in Fig. 3c, f, i, respectively. These results show that the pressure, velocity, and temperature fields display similar variation for all three radii of curvature of the convex substrate. It is observed that the distributions of the pressure and velocity fields on the spatial substrate are slightly non-uniform. Pressure reaches its maximum value at the center of the convex substrate and then gradually decreases with an increasing radius of convexity. Figure 3b, e, f also show that velocity gradually decreases with a decrease in the radius of the convex substrate. There is a stagnant area near the center of the substrate where the velocity is almost zero. This finding agrees well with the corresponding experimental results. It can be concluded that the pressure reaches its maximum and the velocity reaches its minimum at the center of the convex substrate. This conclusion agrees well with the theoretical analysis and the experimental results. However, Fig. 3c, f, i show that the distribution of temperature on the spatial substrate is nearly uniform. There is no obvious temperature fluctuation over the entire surface of the substrate except for a slightly lower temperature at the edge of the substrate. This finding also agrees well with the observation from experiment. The effectiveness of the new cooling system is thus verified by numerical prediction and experimental observation. The system can provide nearly uniform temperature on the substrate surface, which is vital for uniform growth of CS-NCD thin film.

Figure 4 shows the finite element results of pressure, velocity, and temperature fields for different radii of curvature of the concave substrate (R) (134, 108, and 91 mm). The corresponding visualized pressure distributions are shown in Fig. 4a, d, g, the visualized velocity distributions in Fig. 4b, e, f, and the visualized temperature distribution in Fig. 4c, f, i. These results indicate that the distributions of temperature and mass fields as well as pressure and velocity fields in the concave substrate are similar to those in the convex substrate. The pressure and velocity fields are non-uniform on the concave substrate. The velocity of plasma is the lowest and the corresponding pressure is the greatest in the center of the substrate. Meanwhile, there is an approximately uniform temperature field on the domain of substrate except for a slight change in the edge temperature of the substrate. This simulation prediction also agrees well with theoretical analysis and the results of experiments. But greater fluctuation and reflux occur in the domain of concave substrate than on the convex substrate, which would result in changes in the density distribution of activated carbon atom, hydrogen atom, and hydrocarbon atomic groups. This would exert a negative influence on the growth of CS-NCD film. From the above simulation results, it can be concluded that the curved surface substrate can maintain a nearly uniform temperature with the novel cooling system.

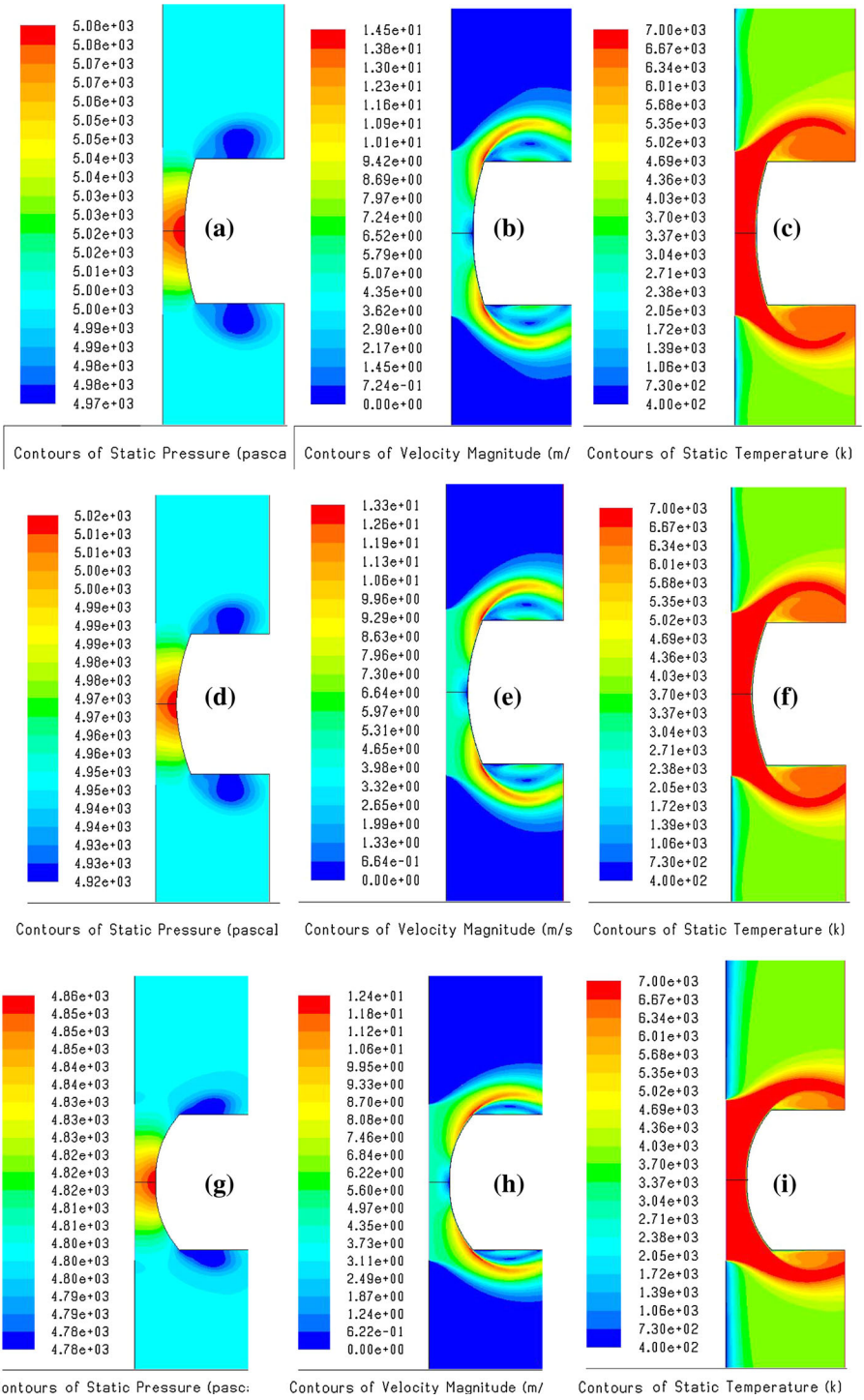

Fig. 3 Fluid field and temperature simulation of convex substrate

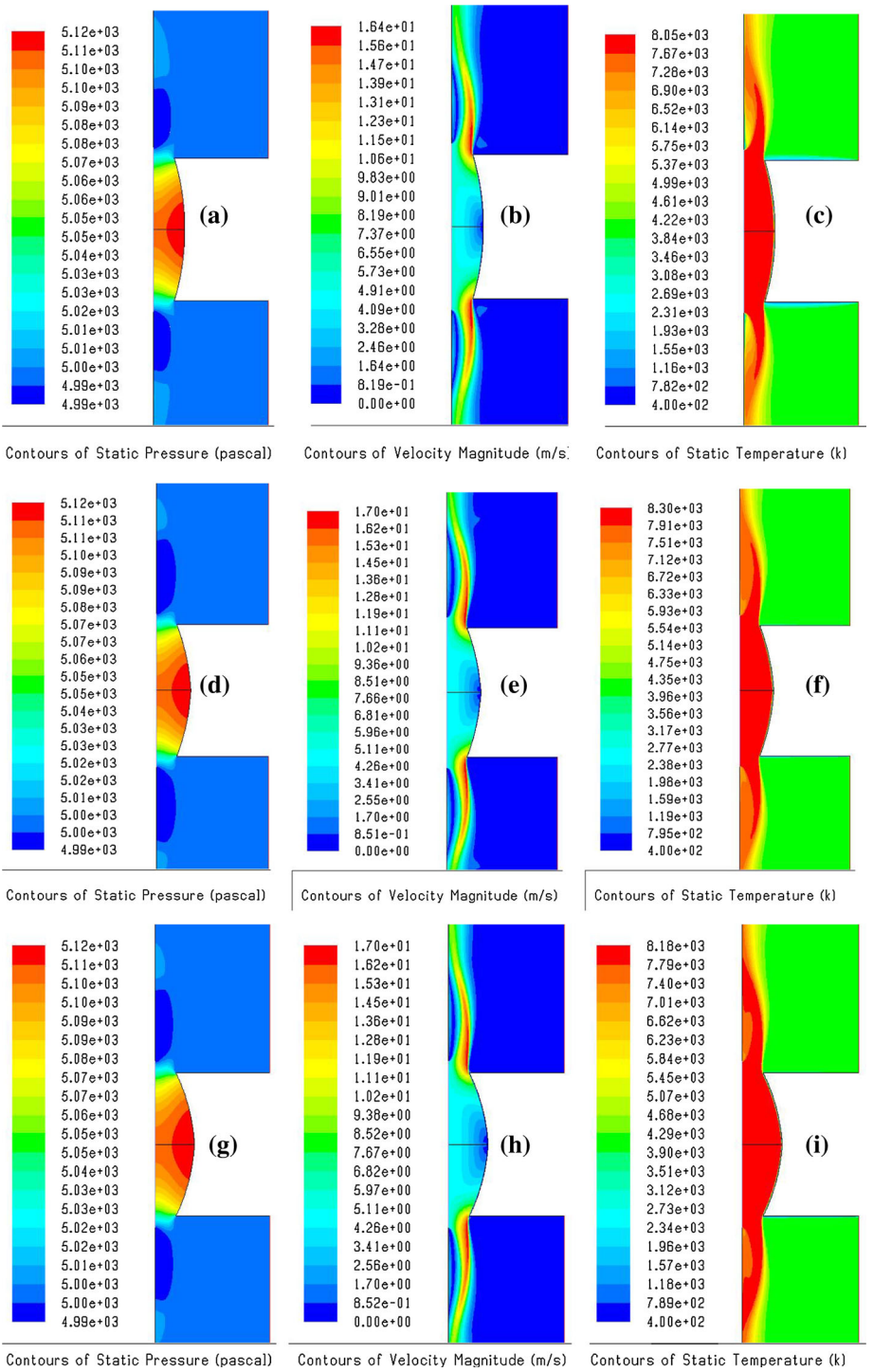

Fig. 4 Fluid field and temperature simulation of concave substrate

Experimental Study

The temperature distribution of the curved surface substrate was also measured in experiment. The results are shown in Tables 2 and 3.

We conducted experiments with five different radii of curvature, namely $R_1 = 134$ mm, $R_2 = 108$ mm, $R_3 = 91$ mm, $R_4 = 78$ mm, $R_5 = 63$ mm, to verify the temperature distribution of the curved surface of the substrate. The results are shown in Table 2, where Ra is a sectional radius of the substrate, and Ra is 32.5 mm. It is found that the temperature difference between the center of the substrate and the edge of the substrate is about 0.6–1.5 %. The distribution of temperature on the convex surface substrate is approximately uniform; thus, the temperature difference of the substrate surface is well controlled by the cooling system. The experimental results agree well with the simulation prediction, and indicate that the novel cooling system is favorable for growing CS-NCD thin films.

The temperature distribution of five different radii of curvature of the concave substrate is shown in Table 3, indicating that the temperature of the center of the substrate surface is 0.8–1.3 % lower than at the edge of the substrate. Using the novel cooling system, the distribution of temperature on the concave surface substrate shows no obvious fluctuation, which is nearly the same as the simulation prediction. A uniform temperature distribution is one of the most important factors for successful preparation of CS-NCD thin films. CS-NCD thin films can be synthesized on either the convex or concave substrate. However, we also find that plasma has superior flow stability on the convex substrate than on the concave substrate, as shown in Figs. 3 and 4. Thus, in this paper, CS-NCD thin films are synthesized on the convex surface substrate.

FE-SEM Analysis

Some FE-SEM images of curved diamond thin films are shown in Fig. 5. FE-SEM seems to be a suitable technology for distinguishing microstructure characterization and the grain

Table 2 Temperature distribution of different radii of the convex substrate in experiment

Measurement points		Experimental parameters	Distance from center of substrate (mm)				
			0 mm	1/4 Ra	1/2 Ra	3/4 Ra	Ra
Chamber pressure: 50–60 Torr, Ar, H_2 and CH_4	Temperature substrate/ °C	Experiment 1	945	941	937	934	931
		Experiment 2	930	927	923	919	916
		Experiment 3	912	908	904	901	898
		Experiment 4	870	867	864	861	859
		Experiment 5	844	841	838	836	833

Table 3 Temperature distribution of different radii of the concave substrate in experiment

Measurement points		Experimental parameters	Distance from center of substrate (mm)				
			0 mm	1/4 Ra	1/2 Ra	3/4 Ra	Ra
Chamber pressure: 50–60 Torr, Ar, H_2 and CH_4	Temperature substrate/ °C	Experiment 1	938	940	943	945	949
		Experiment 2	925	927	930	933	937
		Experiment 3	912	914	917	920	923
		Experiment 4	890	892	894	897	900
		Experiment 5	871	873	876	877	879

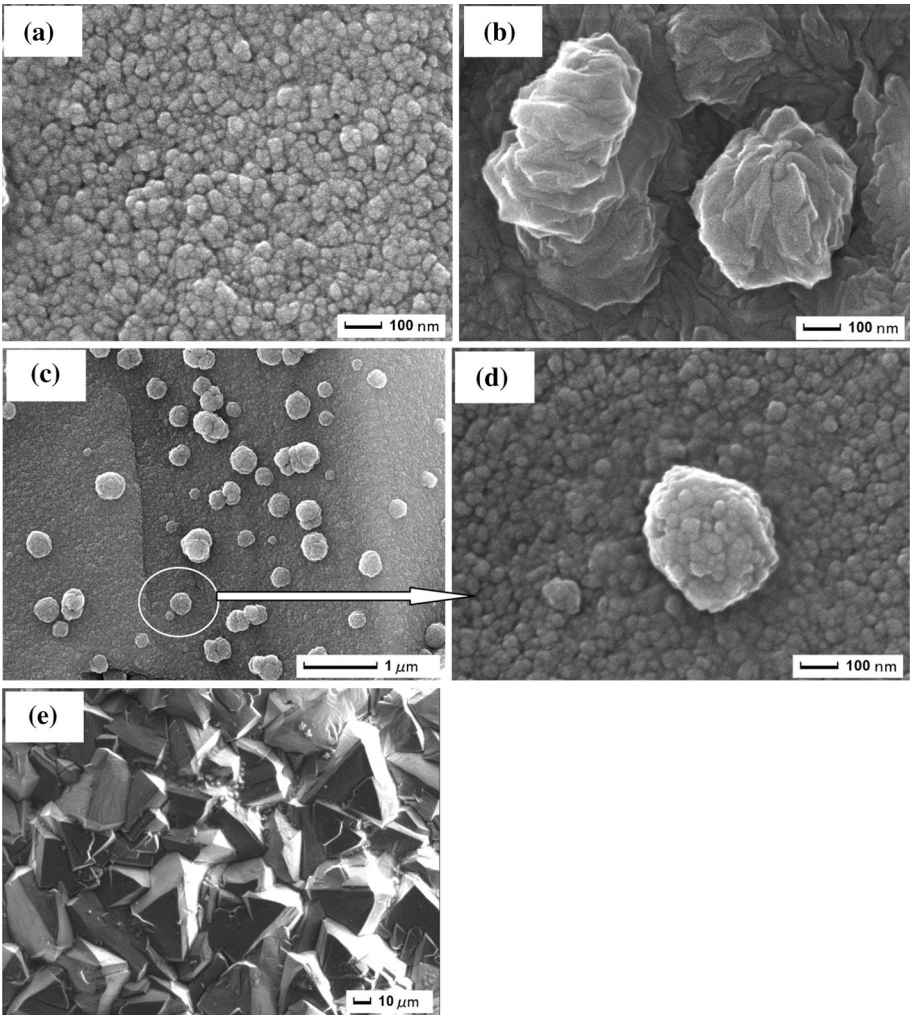

Fig. 5 EF-SEM images of carbon thin films produced by different processes, **a** CS-NCD thin film, CH_4 concentration 4.7 % and substrate temperature 940 °C, **b** secondary growth humps on carbon thin film, CH_4 concentration 4.7 %, substrate temperature 1200 °C, **c** curved surface nanocrystalline-like diamond thin film, CH_4 concentration 8.0 %, substrate temperature 945 °C, **d** enlarged section, **e** curved surface microcrystalline diamond film, CH_4 concentration 1.7 %, substrate temperature 930 °C

size of CS-NCD and non-CS-NCD thin film. Figure 5 compares the Raman spectra of some different representative growth processes.

It can be seen from the visible FE-SEM image shown in Fig. 5a that the CS-NCD thin film was synthesized with CH_4 concentration 4.5 % and substrate temperature 950 °C. It can be observed that the CS-NCD thin film is composed of some nanoclusters and exhibits a flat and compact microstructure. The surface of the film consists of ball-like diamond particles. The reason for the development of this surface might be that, in a high CH_4 concentration, the growth of a non-diamond carbon phase caused secondary nucleation and prevented crystal faceting. The CS-NCD thin film exhibits grain sizes in the range of

20–40 nm in diameter with well-defined grain boundaries. Small grains can be seen in the surface of the CS-NCD thin film. They vary in the range of a few tens of nanometers to twenties of nanometers. Grains are observed to be very smooth, uniform, and there is no appearance of sharp large crystal grains. These results confirm that CS-NCD thin films of about 31 nm grain size can grow on the curved surface substrate.

Figure 5b shows a FE-SEM image of a curved surface diamond film synthesized with CH_4 concentration 4.5 % and substrate temperature 1,200 °C. It is evident that there are some secondary growth humps on the surface of the diamond film. Those humps extend to the interior of the film and present floccus and lack of orientation. The hump size is approximately 200–400 nm. This film differs significantly from both microcrystalline and NCD films. Thus it is evident that substrate temperature is an important growth process parameter, as even at the same CH_4 concentration, it is possible to synthesize different carbon films which cannot grow CS-NCD thin films if the substrate temperature is too high, as in Fig. 5b.

Figure 5c shows that when the methane concentration is 8 % and the curved surface substrate temperature is 940 °C, the surface grains of the diamond film synthesized are <1 micron and at nano-level, thus indicating that CS-NCD thin film has been synthesized. Yet there are some large sharp grain groups on the surface of the diamond film. A particular part of the surface is enlarged and shown in Fig. 5d. The surface grains are about 20 nm, but the size of the large raised grain group is nearly 200 nm. These large raised grain groups are deleterious to the properties of diamond film, resulting in more residual stress, increased surface roughness, low and non-uniform wave-transparency. The reason for the appearance of outstanding grain groups in the second nucleation surface is probably that when diamond film grows under a much higher CH_4 concentration, after the second nucleation there is still a large number of activated carbon atoms and carbon atom groups. These groups grow more rapidly in a favorable position than the surrounding grains, resulting in a third nucleation in the secondary nucleation surface.

The synthetic curved surface thin diamond film shown in Fig. 5e was grown when the methane concentration is 1.7 % and the substrate temperature is 920 °C. Figure 5e reveals clearly the surface morphology of the diamond film, showing (111) faces growing up toward the film surface. This formation dominates the whole surface of the film. The grain size varies in the range of 10–30 micron. Curved surface microcrystalline diamond film is deposited. The grains are uniform and compact, but it is seen that the surface of the micron diamond film is rougher than that of NCD film. Thus, when the CH_4 concentration is as low as 1.7 %, it is difficult to grow CS-NCD thin film. Possible reason is that that under low CH_4 concentration, after the carbon atoms are activated, carbon atom groups adsorb on the nucleation surface and are very quickly incorporated into the lattice of the surface atoms. No atoms remain with the opportunity to nucleate again. Secondary nucleation does not usually occur. The grains grow rapidly along the direction of favorable growth and become very coarse, presenting a particular crystal plane feature.

Previous studies have shown that the growth of CS-NCD thin films may contain a significant proportion of amorphous or non-sp^3 hybridized carbon atoms at grain boundaries, and the nanocrystalline phase results from the insertion of carbon dimers into carbon–carbon and carbon–hydrogen bonds, leading to heterogeneous nucleation rates of the order of 10^{10} cm^2 s^{-1} [28].

AFM Analysis

Atom force microscopy (AFM) can effectively characterize a 3D profile of the surface. On that basis, CS-NCD thin films like that shown in Fig. 5a were investigated by AFM.

Figure 6 shows a typical AFM image of the surface morphology of a CS-NCD thin film grown with $Ar/H_2/CH_4$ plasma jet CVD. The image shows that the microstructure morphology of the synthetic CS-NCD thin film is compact, and the small grain size is uniform. It is also observed that the surface of the samples is characterized by a granular structure, in which no prominent faceted orientation can be found. The granular segments of around 50–200 nm in diameter are embedded in the film. The grain size of these CS-NCD thin films is measured in a range of 22–39 nm. The AFM image of CS-NCD thin film also shows an average particle size of about 30 nm, and it is consistent with that in Fig. 5.

Surface Roughness Profile Study

The surface roughness profile of CS-NCD thin films is plotted in Fig. 7a, b. The figures displays the mean surface roughness [root-mean-square (RMS)] of the diamond films measured over an area of 3,500 nm × 3,500 nm. The mean surface roughness over the central area and the fringe area of CS-NCD thin films is shown in Fig. 7a, b respectively. The mean surface roughness (RMS) of the central area is measured at 4.2 nm, and the RMS over the fringe area is about 4.4 nm. From the experiments there are no obvious spatial dimensional changes in the CS-NCD thin films. The whole surface of the CS-NCD thin films is found to be quite uniformly distributed and flat, which presents a high surface roughness.

Wang et al. [29] found that mean surface roughness is one of the most critical parameters influencing the optical properties of diamond thin films, and CS-NCD thin film is an ideal material for optical applications. Furthermore, due to its high hardness, high gain density and low surface roughness, CS-NCD thin film is a promising material for application in high-precision polishing machining [30].

Raman Spectrum Study

Raman spectroscopy has become one of the most effective techniques for characterizing disordered polycrystalline graphitic carbons. The wavelength of a 514.5 nm argon laser Raman spectrum was used to investigate the full width at half maximum of the peak and

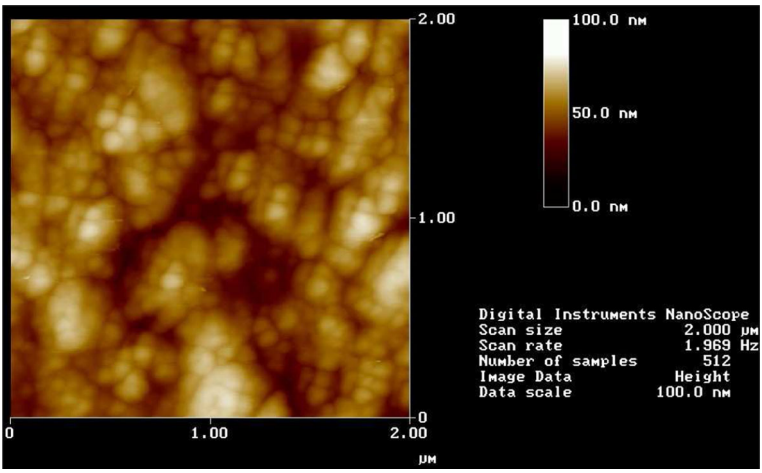

Fig. 6 AFM image of surface morphology of CS-NCD thin film

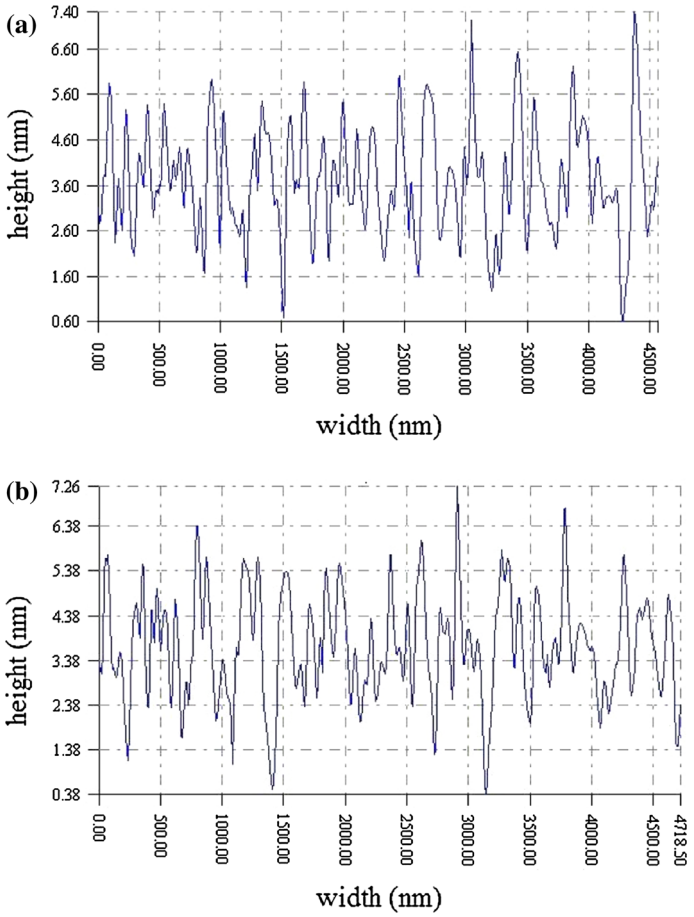

Fig. 7 Surface roughness of CS-NCD thin film: **a** central area, **b** fringe area

the detailed bonding structure of carbon films. The Raman spectra of CS-NCD and non-CS-NCD thin films deposited on the non-spherical surface of a Mo substrate are shown in Fig. 8. The center and the fringe of the CS-NCD thin films are characterized by Raman spectra, which aim to analyze the quality of the entire CS-NCD thin films, shown in Fig. 8a, b, respectively. In Fig. 8a some Raman peaks are observed at 1,145, 1,333, 1,355, 1,495 and 1,555 cm^{-1} in the central area of the thin film. These peaks are almost identically observed at 1,142, 1,334, 1,357, 1,491 and 1,555 cm^{-1} in the fringe area of the thin film, as shown in Fig. 8b. A broadened spectrum is observed, with several peaks in the neighborhood of sp^3 diamond bonding centered around 1,332 cm^{-1}. Raman spectra of CS-NCD thin films such as 1,355, 1,357 cm^{-1} are near 1,350 cm^{-1}, and 1,555, 1,355 cm^{-1} are near 1,580 cm^{-1}, which are commonly known as D and G bands, respectively. They are related to graphitic islands and amorphous carbon. The Raman is more sensitive to non-diamond phase than to diamond phase.

The peaks centered around 1,145, 1,142 cm^{-1} (near 1,140 cm^{-1}) and 1,491, 1,495 cm^{-1} (near 1,480 cm^{-1}), as shown in Fig. 8a, b are considered to be attributed to trans-polyacetylene lying in the grain boundaries, and to bear no relation to C–C (sp^3)

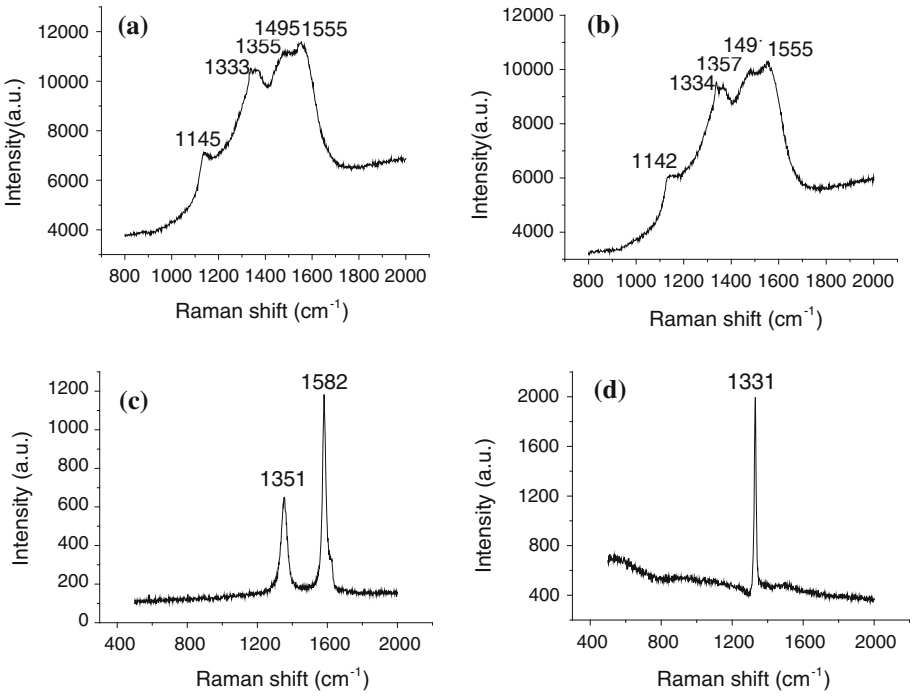

Fig. 8 Raman spectra of CS-NCD and non-CS-NCD carbon thin films, **a** central area of CS-NCD thin film, CH_4 concentration 4.7 %, substrate temperature 940 °C, **b** fringe area of CS-NCD thin film, CH_4 concentration 4.7 %, substrate temperature 940 °C, **c** graphitic islands and amorphous carbon, CH_4 concentration 4.7 %, substrate temperature 1,200 °C, **d** curved surface microcrystalline diamond film, CH_4 concentration 1.7 %, substrate temperature 930 °C

vibrations [31]. These peaks were also observed in the work of [32]. They are related to the calculated phonon density of states of diamond and have been attributed to the presence of nanocrystalline phase of diamond [33]. Raman spectra reveal that sp^3 and sp^2 hybridized C atoms coexist in the films. It is difficult, however, to determine the ratio information quantitatively. Further, residual stress in CS-NCD thin film possibly results in slight fluctuations of peak in the central and fringe areas.

The Raman spectrum of a secondary growth in carbon thin film produced when the CH_4 concentration was 4.7 % and the substrate temperature 1,200 °C is shown in Fig. 8c. It is clearly shown that Raman peaks occur at 1,351 and 1,582 cm^{-1}, which are usually designated as the D peak for graphite and the G peak for amorphous carbon. The double peak structure of D and G is due to the large number of C–C sp^2 phase in the carbon measured Raman spectra. It does not appear at the 1,332 cm^{-1} peak, which is a characteristic peak of the C–C sp^3 phase of diamond, meanwhile, it is not found at the 1,140 and 1,480 cm^{-1} peaks in the carbon film, which are closely related to NCD film. Thus, synthetic carbon film is neither NCD thin film nor microcrystalline diamond thin film in the growth process. It is compared with CS-NCD thin film in Fig. 8a, b. Although at the same CH_4 concentration, too high a temperature on the substrate, as shown in Fig. 8c, grows only non-diamond phase. It is known that diamond thin film is synthesized within a specific temperature range. If the substrate temperature is too high or too low, it results in the formation of amorphous carbon and graphite phase and does not deposit diamond phase.

Figure 8d shows the Raman spectrum of curved surface diamond thin film at CH_4 concentration 1.7 % and substrate temperature 930 °C. A characteristic peak at 1,331 cm^{-1} is found in the Raman spectrum. This is identified as diamond phase due to the sharp peak at 1,332 $cm^{-1.}$ Residual stress in diamond film makes the diamond peak shift at 1,331 cm^{-1}. However, no significant characteristic peaks at 1,350 and 1,580 cm^{-1} originating from disordered graphitic phases and amorphous carbon are observed in Fig. 8d, indicating that curved surface diamond thin film has been successfully synthesized. Meanwhile, the two characteristic peaks of NCD thin film at approximately 1,140 and 1,480 cm^{-1} appear absent. Thus, in a low CH_4 concentration, despite a suitable temperature for growth, there is no synthesis of CS-NCD thin film. This evidence, combined with Fig. 8e, indicates that the synthetic curved surface diamond thin film is micron-crystalline.

From the above analysis of Raman spectra, it can be concluded that CS-NCD components may include amorphous carbon and graphitic islands and may be deposited on non-spherical surface substrates.

Conclusion

Curved surface NCD thin films with a mean grain size of 30 nm were successfully synthesized on a curved surface Mo substrate by DCPJCVD using a gas mixture of Ar, H_2 and CH_4. Based on a novel cooling system, the technique used in this work is flexible and efficient for depositing CS-NCD thin film on a non-flat surface. Diamond nucleations uniformly distribute and assemble on curved surface Mo substrate, under stable plasma source, then harmoniously grow. Experimental study and simulation prediction show that, with the cooling system, a uniform temperature distribution can be obtained on the curved surface substrate. CS-NCD thin films can only be synthesized with certain growth processes. AFM, FE-SEM, Raman and roughness-profile meter observations show that the CS-NCD thin films produced are smooth, uniform, and continuous. The surface roughness of the CS-NCD thin films is about 4.3 nm, with negligible dimensional changes in whole CS-NCD thin films. Raman spectra show some similar features near 1,140 and 1,480 cm^{-1} in the central area and fringe area of diamond films. It is proved that the diamond thin films prepared are CS-NCD thin films. It is also found that the CS-NCD thin film contains little non-diamond phase.

Acknowledgments This project was supported by the Natural Science Foundation of China (51075211, 51275230), Education Science Foundation of Jiangxi Province (GJJ13492) and Doctoral Foundation of NCHU (EA200901168).

References

1. Zeb S, Qayyum A, Sadiq M, Shafiq M, Waheed A, Zakaullah M (2007) Plasma Chem Plasma Process 27:127
2. Henderson MR, Gibson BC, Ebendorff-Heidepriem H, Kuan K, Afshar VS, Orwa JO, Aharonovich I, Tomljenovic-Hanic S, Greentree AD, Prawer S, Monro TM (2011) Adv Mater 23:2806
3. Haggerty SE (2002) Science 297:1531
4. May PW (2008) Science 319:1490
5. Li D, Zuo D, Lu W, Chen R (2008) Solid State Ionics 179:1263
6. Popov C, Kulisch W, Bliznakov S, Mednikarov B, Spasov G, Pirov J (2007) Appl Phys A 89:209
7. Novotný M, Jelínek M, Bulíř J, Lančok J, Vorlíček V, Bonarski J (2004) Appl Phys A 79:1267
8. Wang WL, Sánchez G, Polo MC, Zhang RQ, Esteve J (1997) Appl Phys A 65:241

9. Amaral M, Mohasseb F, Oliveira FJ, Benedic F, Silva RF, Gicquel A (2005) Thin Solid Films 482:232
10. Mochalin VN, Shenderova O, Ho D, Gogotsi Y (2012) Nat Nanotechnol 7:11
11. Okuchi T, Ohfuji H, Odake S, Kagi H (2009) Appl Phys A 96:833
12. Zhou H, Watanabe J, Miyake M, Ogino A, Nagatsu M, Zhan R (2007) Diam Relat Mater 16:675
13. Meng XM, Askari SJ, Tang WZ, Hei LF, Wang FY, Jiang CS (2008) Vacuum 82:543
14. Morell G, Gonzalez-Berrios A, Weiner BR, Gupta S (2006) J Mater Sci: Mater Electron 17:443
15. Shikata S, Fujii S, Sharda T (2005) Diam Relat Mater 18:253
16. Huang SM, Hong FC (2006) Surf Coat Technol 2006(200):3151
17. Lunn B, Wright DA, Zhang LY (1998) Diam Relat Mater 7:129
18. Li D, Zuo D, Zhou X, Hua X (2011) Synth React Inorg M 41:245
19. Grujicic M, Lai SG (1999) J Mater Sci 34:7
20. May PW, Harvey JN, Allan NL, Richley JC, Mankelevich YA (2010) J Appl Phys 108:014905
21. Zuo D, Li D, Lu W, Chen R, SunY (2011) Chinese Patent No. 200810024384.5
22. Li D, Zhou X, Zuo D, Zou A (2012) J Comput Theor Nanosci 9:1511
23. Wang FJ (2004) Computational fluid dynamics analysis-CFD software principles and applications. Tsinghua University Press, Beijing, China
24. ANSYS. Inc., ANSYS, 2012, http://www.ansys.com
25. Qin QH (2000) The trefftz finite and boundary element method. WIT Press, Southampton, England
26. Qin QH (2005) Appl Mech Rev 58(316):316
27. Qin QH, Wang H (2008) Matlab and C programming for Trefftz finite element methods. CRC Press, Boca Raton
28. Gruen DM (1999) Rev Mater Sci 29:211
29. Wang SG, Zhang Q, Yoon SF, Ahn J, Wang Q, Yang DJ (2003) Opt Mater 24:509
30. Li D, Zuo D, Chen R, Xiang B, Lu W, Wang M (2008) Synth React Inorg M 38:325
31. Lopez-Rios T, Sandre E, Leclercq S, Sauvain E (1996) Phys Rev Lett 76:4935
32. Pfeiffer R, Kuzmany H, Knoll P, Bokova S, Salk N, Gunther B (2003) Diam Relat Mater 12:268
33. Miyake M, Ogino A, Nagatsu M (2007) Thin Solid Films 515:4258